Journal of Peptide Science
J. Peptide Sci. **9**: 729–744 (2003)
Published online in Wiley InterScience (www.interscience.wiley.com). DOI: 10.1002/psc.495

JOURNAL OF PEPTIDE SCIENCE

Crystal Structure and Conformational Analysis of Ampullosporin A‡

MATTHIAS KRONEN,[a] HELMAR GÖRLS,[b] HOAI-HUONG NGUYEN,[c] SIEGMUND REIßMANN,[c]* MARTIN BOHL,[d,e] JÜRGEN SÜHNEL,[d]* and UDO GRÄFE[a]§

[a] Hans-Knöll-Institut für Naturstoff-Forschung, Beutenbergstraße 11, D-07745 Jena, Germany
[b] Institut für Anorganische und Analytische Chemie, Friedrich-Schiller-Universität Jena, Lessingstr. 8, 07743 Jena, Germany
[c] Institut für Biochemie und Biophysik, Friedrich-Schiller-Universität Jena, Philosophenweg 12, 07743 Jena, Germany
[d] Institut für Molekulare Biotechnologie, Beutenbergstraße 11, D-07745 Jena, Germany
[e] Tripos GmbH, Martin-Kollar-Str. 17, D-81829 Munich, Germany

Revised 25 April 2003
Accepted 29 April 2003

Abstract: Ampullosporin A is a 15-mer peptaibol type polypeptide that induces pigment formation by the fungus *Phoma destructiva*, forms voltage-dependent ion channels in membranes and exhibits hypothermic effects in mice. The structure of ampullosporin A has been determined by x-ray crystallography. This is the first three-dimensional (3D) structure of the peptaibol subfamily SF6. From the *N*-terminus to residue 13 the molecule adopts an approximate right-handed α-helical geometry, whereas a less regular structure pattern with β-turn characteristics is found in the *C*-terminus. Even though ampullosporin A does not contain a single proline or hydroxyproline it is significantly bent. It belongs to both the shortest and the most strongly bent peptaibol 3D structures. The straight structure part encompasses residues Ac-Trp^{1}-Aib^{10} and is thus less extended than the α-helical subunit. The 3D structure of ampullosporin A is discussed in relation to other experimentally determined peptaibol structures and in the context of its channel-forming properties. As a part of this comparison a novel bending analysis based on a 3D curvilinear axis describing the global structural characteristics has been proposed and applied to all 3D peptaibol structures. A sampling of 2500 conformations using different molecular dynamics protocols yields, for the complete ampullosporin A structure, an α-helix as the preferred conformation *in vacuo* with almost no bend. This indicates that solvent or crystal effects may be important for the experimentally observed peptide backbone bending characteristics of ampullosporin A.

Keywords: peptaibol; ampullosporin A; crystal structure; ion channel; molecular dynamics; conformational analysis; bending analysis

Abbreviations: 3D, three-dimensional; CSD, Cambridge Structural Database; MD, molecular dynamics; PDB, Protein Data Bank.
Data deposition: The atomic coordinates have been deposited at the Cambridge Crystallographic Data Centre, 12, Union Road, Cambridge CB2 1EZ, UK (accession no. CCDC 195231).

* Correspondence to: Professor Siegmund Reißmann, Friedrich-Schiller-Universität Jena, Institut für Biochemie und Biophysik, Philosophenweg 12, D-07743 Jena, Germany; e-mail: reissmann@merlin.biologie.uni-jena.de for experimental aspects or to Dr. Jürgen Sühnel, Institut für Molekulare Biotechnologie, Beutenbergstraße 11, D-07745 Jena, Germany; e-mail: jsuehnel@imb-jena.de

‡ Presented at Peptaibols, October 2002, Jena, Germany.

§ deceased.

INTRODUCTION

Peptaibols are polypeptides that are characterized by the presence of the unusual amino acid 2-aminoisobutyric acid (Aib). In addition, they have an acetylated *N*-terminus and a *C*-terminal amino alcohol. Their sequence length is in the range 5–20 and they often contain further modified amino acids such as isovaline (Iva) and hydroxyproline (Hyp). Most peptaibols form helical structures and are able to self-associate thereby forming ion-conducting pores in artificial membranes [1].

Thus far, three-dimensional (3D) peptaibol structures have been reported for alamethicin (x-ray structure, three chains in asymmetric unit; PDB code: 1AMT [2]), antiamoebin I (x-ray structure, two chains in asymmetric unit, PDB code: 1JOH [3]; x-ray structure, one chain in asymmetric unit, CSD code: FEJQOA [4]), chrysospermin C (NMR average structure, PDB code: 1EE7 [5]), trichotoxin_A50E (x-ray structure, two chains in asymmetric unit, PDB code: 1M24 [6]), zervamicin IIB (NMR structure, 20 models, isotropic solvent, PDB code: 1DLZ [7]; NMR structure, 20 models, bound to dodecylphosphocholine micelles, PDB code: 1IH9 [8]), [Leu^1]zervamicin (x-ray structure, one chain in asymmetric unit, CSD code: KIYPUD [9]). When finalizing this manuscript the NMR solution structure of antiamoebin I was published (PDB code: 1GQ0) [10]. The structures of trichogin A IV [11] and of trichorzianin TA VII [12] have also been resolved. However, in the latter two cases, the full sets of 3D coordinates have not been made publicly available. All peptaibol 3D structures currently known exhibit a bend of different extent.

A comprehensive collection of peptaibol sequences as well as of 3D structures is provided by the Peptaibol Database hosted by the Crystallography Department of Birkbeck College, London www.cryst.bbk.ac.at/peptaibol/. Recently, an alignment of the over 200 peptaibol sequences was used to define nine peptaibol subfamilies (SFs) [1].

Ampullosporin A, a peptaibol-type fungal antibiotic, was isolated from *Sepedonium ampullosporum*. It was reported to promote pigment formation by the fungus *Phoma destructiva*, to induce hypothermia in mice and to inhibit their locomotor activity suggesting a neuroleptic effect [13]. Specific neuropharmacological tests confirmed that ampullosporin A can act as an atypical antipsychotic drug (Greksch, personal communication). Further, ampullosporin A was found to form pores or channels in artificial membranes [14]. Several related structures such as the homologous ampullosporins B–E [15] and a series of synthetic and semisynthetic analogues [16,17] showed biological activities as strong as ampullosporin A [13,15,17]. Recently, a correlation between the membrane activities of ampullosporin-type peptaibols and their biological activities has been suggested Grigoriev *et al*, personal communication).

Ampullosporin A is a typical peptaibol with an acetylated *N*-terminus, seven Aib units in the total sequence of 15 amino acids and an amino alcohol (leucinol) at the *C*-terminus. In contrast to many other peptaibols it contains neither a proline nor a hydroxyproline. The sequence is:

Ac-L-Trp^1-L-Ala^2-Aib^3-Aib^4-L-Leu^5-Aib^6-L-Gln^7-Aib^8-Aib^9-Aib^{10}-L-Gln^{11}-L-Leu^{12}-Aib^{13}-L-Gln^{14}-L-Leu^{15}-ol

Ampullosporin is a member of the peptaibol subfamily SF6, for which no 3D structure has been reported thus far. Here the x-ray structure of ampullosporin A and the results of a comprehensive theoretical conformational analysis are presented. In addition, a new method is described for quantitative analysis of the bending geometry and this method is applied to the currently known 3D peptaibol structures listed above and to the most stable ampullosporin conformation found in the theoretical conformational analysis. Finally, possible implications for ion-channel formation are discussed.

MATERIALS AND METHODS

X-Ray Diffraction

Ampullosporin A was isolated from cultures of *Sepedonium ampullosporum* by means of chromatographic methods as previously described [13]. Crystals were grown from an acetonitrile solution. Ampullosporin A was first dissolved in hot solvent. The solution was cooled slowly whereby crystals precipitated. The x-ray diffraction data were collected on a Nonius KappaCCD diffractometer, using graphite-monochromated Mo-K_α radiation. The data were corrected for Lorentz and polarization effects [19,20,21]. The structure was solved by direct methods (SHELXS) [21] and refined by full-matrix least squares techniques against Fo^2 (SHELXL-97) [22]. For all amino and hydroxyl groups, and for the water molecules, the hydrogen atoms were located

by difference Fourier synthesis and refined isotropically. All other hydrogen atoms were included at calculated positions with fixed thermal parameters. The non-hydrogen atoms were refined anisotropically [21]. XP (SIEMENS Analytical X-ray Instruments, Inc.) was used for structure representations. Details of the structure determination are reported in Table 1.

Table 1 Crystallographic Data and Details of Data Collection and Refinement of Ampullosporin A

Chemical formula	$C_{77}H_{127}N_{19}O_{19} * C_2H_3N * 2H_2O$
Molecular weight [$g \cdot mol^{-1}$]	1700.06
Crystal dimension [mm^3]	$0.12 \times 0.12 \times 0.10$
Crystal habit	Colourless prism
Crystal system	Monoclinic
Space group	$P2_1$ (No. 7)
λ [Å]	0.71073
Temperature [K]	183
Unit cell dimensions	
a [Å]	19.9914(4)
b [Å]	9.9246(3)
c [Å]	25.4809(5)
β [°]	111.572(1)
Cell volume [$Å^3$]	4701.5(2)
No. of formula units Z	2
Density (calculated) D_c [$g \times cm^{-3}$]	1.201
Absorption coefficient μ (Mo K_α) [cm^{-1}]	0.88
2Θ range [°]	3.32–55.06
Resolution [Å]	0.77
Completeness [%]	98.6
Unique total data	18190
Observed data with $I > 2\sigma(I)$	12835
No. of variables/restraints	1177/1
R [$I > 2\sigma(I)$][a]	R1 = 0.0512
	wR2 = 0.1294
R (all data)[a]	wR1 = 0.0747
	wR2 = 0.1390
Goodness-of-fit	0.901
Largest diff. peak and hole [$eÅ^{-3}$]	0.758/−0.351
Temperature factors U_{eq}[$Å^{-3}$]	
Carbon atoms	0.035–0.167
Oxygen atoms	0.041–0.118
Nitrogen atoms	0.036–0.089

[a] $R1 = [\Sigma||F_o| - |F_c||]/\Sigma|F_o|$, $wR2 = [[\Sigma w(|F_o^2 - F_c^2|)^2]/[\Sigma w(F_o^2)]]^{1/2}$, $w = 1/[(\sigma F_o)^2 + (aP)^2]$. The value of aP was obtained from structure refinement.

Quantitative Analysis of the Peptaibol Bending Geometry

A uniform method is described for the quantitative analysis of bending geometry of peptaibols that can also be applied to other bent peptide or protein structures. In a first step, a unique 3D curvilinear axis is generated for each peptaibol using an approach implemented in the program P-Curves [23]. In this approach each peptide bond is represented by a local coordinate system with its origin at a characteristic peptide-bond base point (P point). The angle difference between the local axis vectors provides information on the change of direction of the 3D curvilinear axis in passing from one peptide group (n) to the next ($n + 1$).

This local bend angle (Theta angle for Global Axis Curvature in P-curve output) is used to define an N-terminal straight part of the peptaibol structures by assuming that it is characterized by consecutive local bend angles each one being smaller than 9°. Then a least-squares straight-line axis is determined for this structure part again using P-Curves. In a next step, the straight portion of the 3D curvilinear and the straight-line axes are superimposed starting from the N-terminus. Two different quantities are determined on the basis of this superposition by using a SYBYL [24] script: (i) the shortest, i.e. perpendicular, distances between the P points on the 3D curvilinear axis and the straight-line axis as well as (ii) the displacement of P point projections along the straight-line axis relative to the projection of the first N-terminal P point. These two quantities form the axes of a novel two-dimensional (2D) bending graph. Another perspective to understand this new 2D bending graph is to consider the individual residue deviations from a linear molecular axis and to rotate those offsets separately around the straight axis into a common 2D plane, thereby lowering the dimensionality of the structure description from 3D to 2D.

There are several ways in which one could measure the bending properties of these peptides, for example with an average perpendicular distance per structure or, as often used, with a single-parameter bending angle determined either by using atoms subjectively selected or by fitting a kinked line consisting of two straight segments to the 3D curvilinear axis. Some of such bending measures take the different lengths of the linear structure sections into account, others do not. The 2D bending graphs are used as a simple basis for deriving bending information in a relatively consistent way. Keep in mind that all bending quantities, including ours, will be affected by several

factors such as the somewhat subjective definition of the straight segments, the not exact planarity of the 3D curvilinear axes, structural variations represented by different chains or models of one given peptide etc. Therefore, angle ranges rather than single values are presented.

Note, that similar 2D graphs could also be generated for C_α atoms or for any other set of peptide atoms instead of P points as reference. Such 2D graphs would mix bending information as quantified above with the additional deviation of the chosen reference atoms from the 3D curvilinear backbone axis.

As already noted the 2D bending graph provides clear information as to whether or not the two sufficiently straight segments necessary for a bending angle determination are indeed present in the given structures. Also, it should be noted that small differences in the *N*-terminal 3D structure part may affect the orientation of the straight-line axis and, accordingly, influence all distances in the 2D bending graph and thus also the bending angle.

A more detailed description of the approach and results not presented here for the sake of brevity are available from the website www.imb-jena.de/peptaibols/. A SYBYL script using SPL (SYBYL Programming Language) calculates the perpendicular distances and displacements for the 2D bending graph and can be obtained from the authors upon request.

Conformational Sampling

A comprehensive analysis was performed of the conformational space of ampullosporin A. α-Helix and 3_{10}-helix conformations of ampullosporin A were constructed using the SYBYL molecular modelling software version 6.7 using the bigpro biopolymer dictionary [24]. The geometry of both starting conformations was optimized using the Weiner *et al.* all-atom force field as implemented in the SYBYL software (Tripos, Inc.) [25,26]. As the 3_{10}-helix was found to be energetically disfavoured relative to the α-helix, it was taken as the starting point for two different, unbiased and unconstrained *in vacuo* molecular dynamics (MD) simulations using the same force field and respective atomic charges. For a comprehensive analysis of the conformational space results from both simulations were collected. 2000 conformations were extracted from the first MD simulation of 1 ns at 340 K temperature (NTV ensemble, initial Boltzmann velocities, 1 fs interval step, all bonds to shake, no periodic boundary conditions nor any constraints, non-bonded cut-off of 8 Å, non-bonded list update every 25 fs, distance dependent dielectric function). In addition, 500 conformations were obtained from a simulated annealing dynamics (similar parameter settings as above but 0.5 fs interval step, no bonds to shake, exponential anneal function). The simulated annealing protocol was similar to the one used by Krause *et al.* [27]: 2 ps high temperature interval at 700 K followed by a 5 ps annealing interval with exponentially decreasing temperature to 200 K. The geometry of all 2500 structures was subsequently optimized using the Weiner *et al.* all-atom force field with an r.m.s. displacement termination criterion of 0.001 Å and a maximum number of 1000 iterations per structure. All 2500 conformations, the starting conformation and the x-ray crystal structure were stored in a final Molecular Spreadsheet [24]. From these data the 28 backbone torsion angles φ and ψ and the interatomic distance between the C_α atoms of Ac-Trp^1 and Leu^{15}-ol were determined and stored within the molecular structure table. Based on this C_α-C_α distance and on all φ and ψ backbone torsions, a factor analysis (Nipals algorithm, pre-analysis autoscaling, no column filtering, no rotation of axes, no validation) was performed to further analyse the conformational space. Factor or principal component analyses have been used before to investigate and visualize the high-dimensional conformational space [28]. In addition to the factor analysis with backbone torsional angles and the C_α-C_α distance between the *N*-terminal and *C*-terminal amino acids, angles between the peptide-bond planes were used for conformational analysis. AVER_ALPHA and AVER_3_10 were calculated, where the first quantity stands for the average value of all angles between peptide-bond plane (i) and peptide-bond plane (i + 4), and AVER_3_10 represents the average angle between all peptide-bond planes (i) and (i + 3). In the case in which an individual angle was in the range 90°–180°, the smaller complementary angle between 0° and 90° was always chosen. Angles between peptide-bond planes were also used as major criteria to distinguish different types of helices in the new secondary structure assignment programme (Lovell and Cailliez, personal communication). All calculations were performed on a Silicon Graphics Octane R12,000 workstation with 300 MHz and 896 Mbytes main memory running IRIX version 6.5.

RESULTS AND DISCUSSION

Crystal Packing

The packing arrangement of the ampullosporin A crystal depicting both the head-to-tail and the antiparallel side-by-side orientation of the ampullosporin A molecules is shown in Figure 1. The asymmetric unit of the crystal contains only one molecule. In addition, one acetonitrile and two water molecules per ampullosporin are included in the x-ray structure. There are three head-to-tail hydrogen bonds (H-bonds) (Table 2). The first one is formed between the backbone groups NH of Ac-Trp^{1} and CO of Gln^{14}. The two others occur between the backbone NH groups of Ala^{2}, Aib^{3} and the side-chain CO group of Gln^{14}. The side-by-side packing of H-bonded ampullosporin molecules exhibits an anti-parallel orientation (Figure 1). Four H-bonds link the side-chain NH groups of the glutamines 7, 11 and 14 to the backbone carbonyl groups of Ac^{0} and Aib^{10} and to the side-chain carbonyl groups of Gln^{7} and Gln^{11}. From this H-bond pattern and from Figure 1 it is obvious that the two anti-parallel molecules are significantly shifted relative to each other.

Molecular Structure

The intramolecular H-bonds of ampullosporin A are compiled in Table 2 and the torsional angles are given in Table 3. A stereo representation of the x-ray structure is shown in Figure 2. Adopting a donor-acceptor (D···A) distance smaller than 3.5 Å as H-bond criterion, the amino acids 1–13 and also the H-bond between the *N*-terminal acetyl

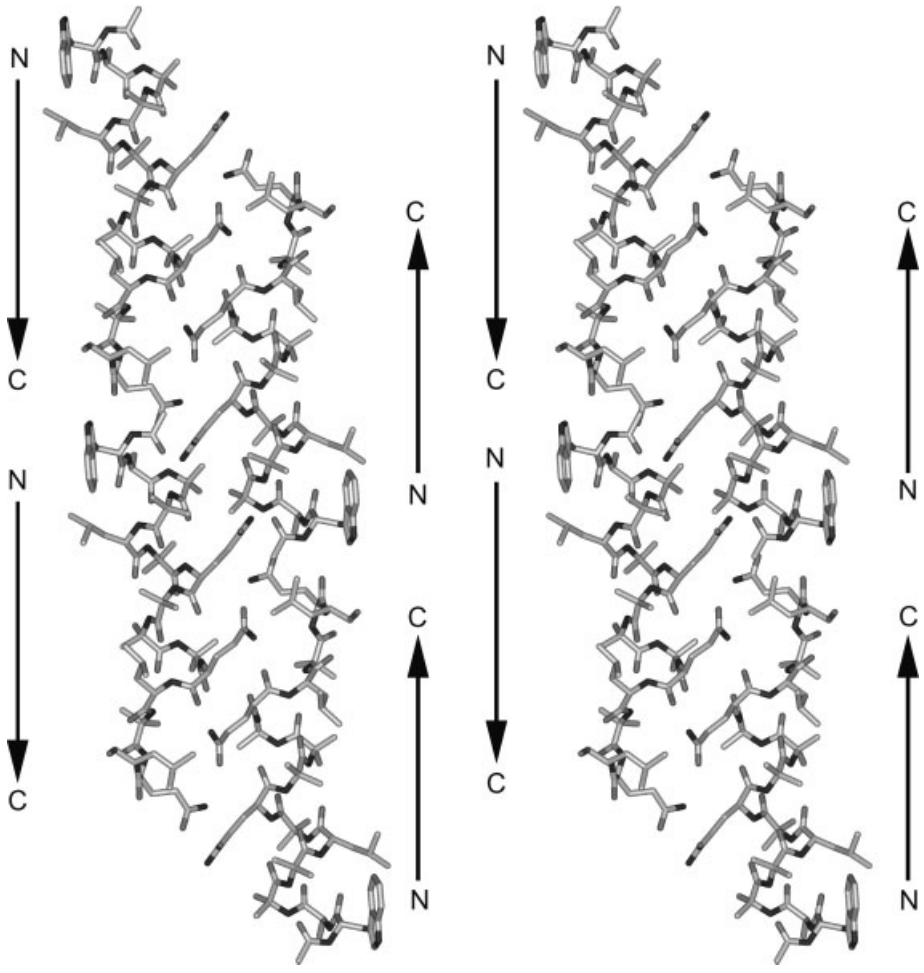

Figure 1 Stereo view of the crystal packing arrangement of ampullosporin A. The figure shows two antiparallel strands consisting each of two head-to-tail linked molecules. N and C stand for the *N*- and *C*-terminus, respectively. Hydrogen atoms and solvent molecules are not displayed.

Table 2 Geometrical Parameters of Intramolecular and Intermolecular Hydrogen-Bond Interactions D–H···A in the Ampullosporin A X-Ray Structure[a]

Type	Donor Atom (D)	Acceptor Atom (A)	Distance D···A (Å)	Distance H···A (Å)	Angle D–H···A (°)
Intramolecular					
i + 4,i	N(Aib^4)	O(Ac^0)	2.918	2.157	168
i + 4,i	N(Leu^5)	O(Ac-Trp^1)	2.954	2.311	155
i + 4,i	N(Aib^6)	O(Ala^2)	3.026	2.247	159
i + 4,i	N(Gln^7)	O(Aib^3)	3.101	2.395	158
i + 4,i	N(Aib^8)	O(Aib^4)	2.844	2.130	173
i + 4,i	N(Aib^9)	O(Leu^5)	3.018	2.201	166
i + 4,i	N(Aib^{10})	O(Aib^6)	3.367	2.702	157
i + 3,i	N(Aib^{10})	O(Gln^7)	3.149	2.740	119
i + 4,i	N(Gln^{11})	O(Gln^7)	3.162	2.523	161
i + 3,i	N(Gln^{11})	O(Aib^8)	3.137	2.714	124
i + 4,i	N(Leu^{12})	O(Aib^8)	2.831	2.059	157
i + 3,i	N(Leu^{12})	O(Aib^9)	3.363	2.863	121
i + 4,i	N(Aib^{13})	O(Aib^9)	3.127	2.474	136
i + 3,i	N(Leu^{15}-ol)	O(Leu^{12})	2.960	2.173	164
Intermolecular					
Head-to-tail	N(Ac-Trp^1)	O(Gln^{14})	2.870	1.968	168
	N(Ala^2)	O$^\varepsilon$ (Gln^{14})	2.863	2.063	154
	N(Aib^3)	O$^\varepsilon$ (Gln^{14})	3.148	2.319	165
Side-by-side	N$^\varepsilon$ (Gln^7)	O(Ac^0)	3.156	2.192	149
	N$^\varepsilon$ (Gln^{11})	O(Aib^{10})	2.897	1.843	171
	N$^\varepsilon$ (Gln^{14})	O$^\varepsilon$ (Gln^7)	2.944	2.016	170
	N$^\varepsilon$ (Gln^{14})	O$^\varepsilon$ (Gln^{11})	2.942	2.039	177
Peptide-solvent					
	N$^\varepsilon$ (Ac-Trp^1)	O(water^2)	2.922	2.064	165
	N$^\varepsilon$ (Gln^{11})	O(water^1)	3.041	2.268	162
Solvent-peptide					
	O(water^1)	O(Gln^{11})	2.766	1.846	160
	O(water^2)	O(Leu^{12})	2.834	1.787	148
	O(water^2)	O(Leu^{15}-ol)	2.845	1.720	177
Solvent-solvent	O(water^1)	N(MeCN)	3.059	2.405	157

[a] Interactions of the type D–H···A are considered as H-bonds if the D···A distance is smaller than 3.5 Å. If one adopts as further H-bond criterion that the H···A distance has to be equal or smaller as 2.5 Å, the total number of intramolecular H-bonds is reduced from 14 to 10.

group and Aib^4 exhibit a H-bond pattern where N-H groups of residue i + 4 and the oxygen of residue i are linked. This pattern is typical for an α-helical structure. However, the structure is definitely not completely regular. First, the α-helical H-bond between Aib^6 and Aib^{10} has an H···A distance substantially larger than 2.5 Å. Moreover, three additional i,i + 3 H-bonds, usually assumed to be indicative for a 3_{10}-helix, are found for the amino acid pairs Gln^7/Aib^{10}, Aib^8/Gln^{11} and Aib^9/Leu^{12}. This means that residues 10–12 form bifurcated H-bonds to residues i − 3 and i − 4, where the angle D–H···A for the i,i + 3 interactions is rather small, however. Also, the H···A distances of these H-bonds are in the range between 2.7 and 2.9 Å and thus longer than 2.5 Å. In addition, there is an i,i + 3 H-bond between Leu^{12} and Leu^{15}-ol. Interestingly, the backbone oxygen atoms of Aib^{10} and Gln^{11} are not involved in intramolecular H-bonds, but are surface exposed instead.

As shown in Table 3 all peptide bonds adopt an approximate *trans*-configuration. For the amino acids 2–10 the torsional angles φ and ψ are in the range of −50° to −72° and −41° to −52°, respectively. Typical torsional angle values are $\varphi = -63°$ and $\psi = -42°$ for α-helices and $\varphi = -57°$ and $\psi = -30°$

Table 3 Backbone (φ, ψ, ω) Torsional Angles of the Ampullosporin A X-ray Structure[a]

Residue	φ (°)	ψ (°)	ω (°)
Ac-Trp^1	−79[b]	−27	174
Ala^2	−64	−51	175
Aib^3	−53	−53	−172
Aib^4	−59	−50	−173
Leu^5	−71	−41	178
Aib^6	−54	−47	−176
Gln^7	−72	−43	177
Aib^8	−50	−48	−175
Aib^9	−57	−52	−178
Aib^{10}	−53	−45	−170
Gln^{11}	−82	−31	−175
Leu^{12}	−94	0	−163
Aib^{13}	−56	−24	176
Gln^{14}	−134	23	176
Leu^{15}-ol	−128		

[a] The torsional angles were calculated with PROMOTIF [30].
[b] Calculated taking into account geometrical information from the acetyl group.

for 3_{10}-helices, respectively. From these data one would conclude that ampullosporin A adopts a relatively regular α-helical structure between Ala^2 and Aib^{10}. The ψ angles for Gln^{11}, Leu^{12} and Aib^{13} could indicate a 3_{10}-helical pattern. Moreover, residues Leu^{12} to Leu^{15}-ol also fulfil the geometrical criteria for a β-turn.

If one takes together H-bond pattern data and backbone torsional angles it turns out that the *N*-terminal part can best be described as an α-helix. There is no clear conclusion about the extension of this α-helical part, however. For the *C*-terminal residues possible classifications are either β-turn or 3_{10}-helix. In view of these partly contradictory results, the secondary structure characteristics of ampullosporin A were determined by applying the program PROMOTIF v. 3.01, which is widely used for protein structures [30]. PROMOTIF identifies 10 out of the 14 intramolecular H-bonds compiled in Table 2 because interactions with an H···A distance larger than 2.5 Å have not been taken into account. PROMOTIF assigns a right-handed α-helix to residues 1–13 and a β-turn to residues 14 and 15.

We are aware of the fact that PROMOTIF is more suitable for the secondary structure determination of larger proteins than for small peptides such as peptaibols. Nevertheless, the PROMOTIF results can be taken as our final assignment. This means that ampullosporin A forms an α-helix for residues 1–13 and exhibits a less regular structure with β-turn characteristics in the remaining two residues at the *C*-terminus. Hence, the rather long H-bond interaction between Aib^6 and Aib^{10} does not prevent an α-helical assignment for the complete residue stretch from 1 to 13. Furthermore, even though there are i,i + 3-type H-bonds in the *C*-terminus, this is obviously not sufficient for a classification as a 3_{10}-helix.

Here, it is important to note that conformational transitions between enantiomeric 3_{10}-helices were found in the crystal structures of poly(Aib) [31]. In addition, the recently solved NMR structure of antiamoebin I exhibits in contrast to the completely right-handed x-ray structure a left-handed helical conformation towards the *N*-terminus [10].

It is well known that tri-, tetra- and pentapeptides containing at least one Aib residue fold into a 3_{10}-helical structure. It is already known, however, that longer Aib-containing peptides have α-helical or mixed $3_{10}/\alpha$-helical geometries, for a review see [32]. In view of these data it is not surprising that the major part of ampullosporin A consists of an α-helix. A similar result was found for the recently solved structure of the 18-residue peptaibol trichotoxin, that contains nine Aib residues [6].

The structure of ampullosporin A, although being quite short in sequence, exhibits a significant bend. Quantitative bending information is displayed in the two-dimensional bending graph (Figure 3). Between Ac-Trp^1 and Aib^{10} the structure is relatively straight. On the other hand, there is no objective way to determine a straight *C*-terminal segment necessary for bending angle determination. If one defines the *C*-terminal straight line by the Aib^{13}/Gln^{14} and Gln^{14}/Leu^{15}-ol peptide-bond base points a bending angle of 63° is obtained. Drawing a straight line through the P points Leu^{12}/Aib^{13} and Gln^{14}/Leu^{15}-ol gives an angle value of 58° and, finally, defining the straight *C*-terminus by the P points Leu^{12}/Aib^{13} and Aib^{13}/Gln^{14} results in a bending angle of 54°. So, assuming a ±1° uncertainty in the angle determination from the straight-line axis and a P point pair, a relatively reliable bending angle range for ampullosporin A should be in the range 53°–64°.

Comparison with Other Peptaibol Structures

In this section the structure of ampullosporin A is discussed in the context of other currently known peptaibol structures, for which coordinates have been deposited at public databases. This

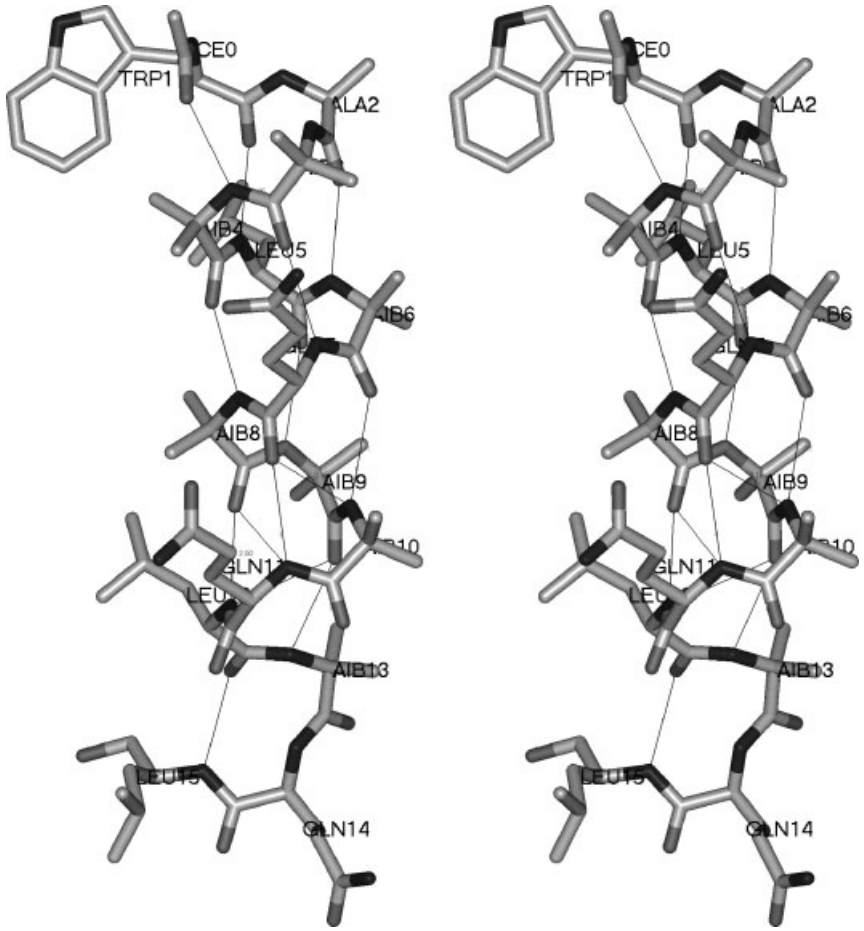

Figure 2 Stereo representation of the ampullosporin A crystal structure (hydrogen atoms and solvent molecules not shown). ACE0 stands for the *N*-terminal acetyl group. The solid lines indicate H-bond interactions, where, however, only the heavy atoms are shown (see column 4 of Table 2).

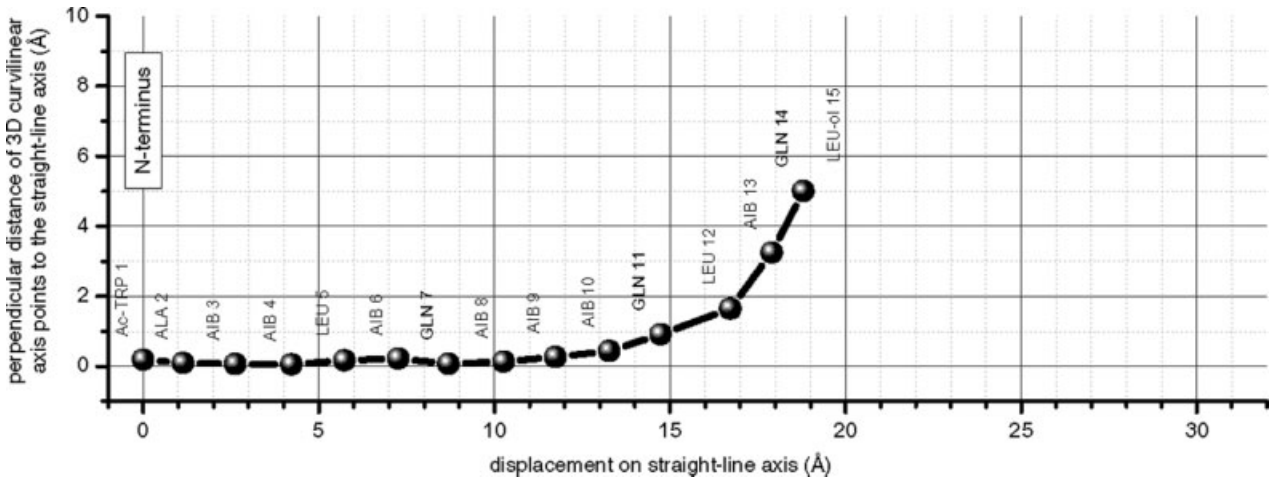

Figure 3 Two-dimensional bending graph for ampullosporin A: the perpendicular distance of peptide-bond base points on the 3D curvilinear axis (spheres) to the straight-line axis obtained from the approximately straight portion between Ac-Trp[1] and Aib[10] versus the displacement of the peptide-bond base point projections along the straight-line axis.

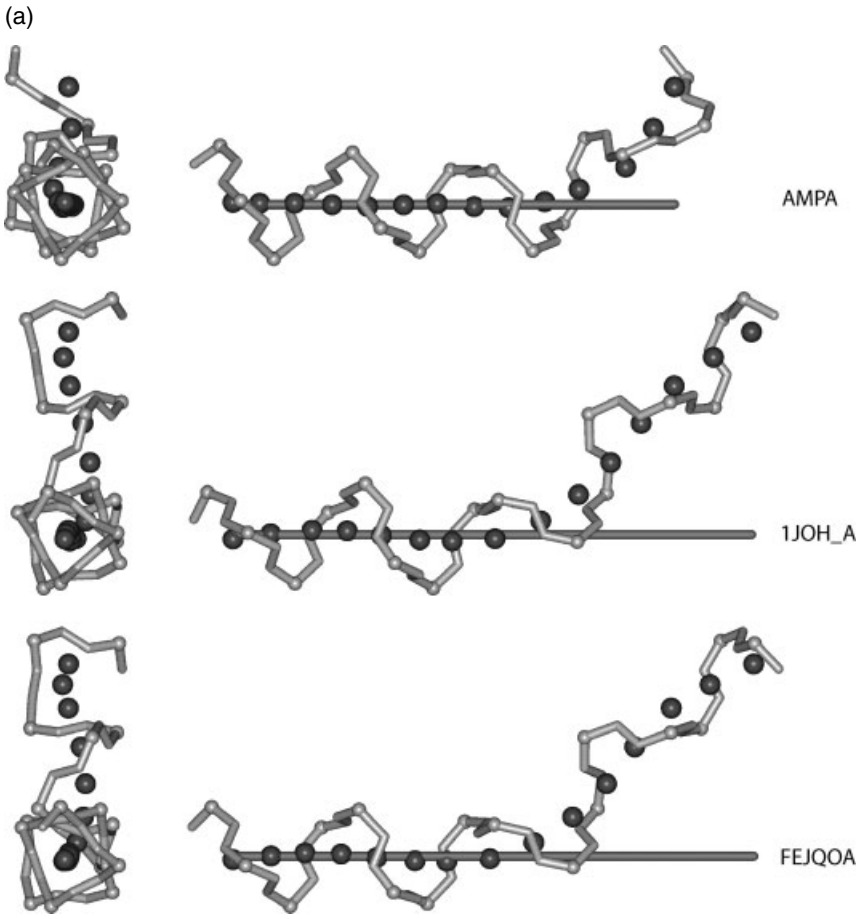

Figure 4a Backbone structure (sticks, Cα atoms: small balls, no oxygen atoms shown), peptide-bond base point of the 3D curvilinear axis (balls) and straight-line axis of peptaibols shown in two orientations rotated by 90°. The database codes are explained in the Introduction.

is done by applying our novel method for the quantitative determination of bending to all of these structures. In Figures 4a, 4b and 4c 3D curvilinear peptide-bond base points, straight-line axes and the backbone structure are shown for ten peptaibol structures both in a side and top view orientation. In Figure 5, a 2D bending graph is shown. All peptaibols are superimposed in this plot with respect to their linear substructures starting at the *N*-terminus. In Table 4 geometrical bending parameters are compiled.

The peptaibol sequence lengths range between 20 for alamethicin and 15 for ampullosporin A. Therefore, ampullosporin A is the shortest peptaibol included in the Table. Note, however, that trichogin A IV, not included in the compilation, has only 11 amino acids and is even shorter than ampullosporin A [11]. The top views in Figure 4 clearly show that the curvilinear 3D axes do not deviate significantly from a plane. An exception is the chain C of 1AMT. Therefore, using the 2D bending graphs for the bending angle determination is justified in almost all cases. The straight *N*-terminal structure parts (Table 4, Figure 5) cover a range of 7 amino acids for zervamicin IIB, [Leu^1]zervamicin and antiamoebin I, over 10 amino acids for chrysospermin C and trichotoxin A50E, to 11 or 12 amino acids for chains A and B of alamethicin. As already noted the bending angle determination requires the selection of two relatively straight structure segments. Straight *N*-terminal segments can easily be determined in a unique manner for all structures shown in Figure 4. The identification of straight *C*-terminal segments is not that simple, however. For antiamoebin I (1JOH, FEJQOA) and for Leu^1 zervamicin (KIYPUD), for example, the *C*-terminal structures are significantly curved and therefore there is no unique way of selecting a straight segment. As already described

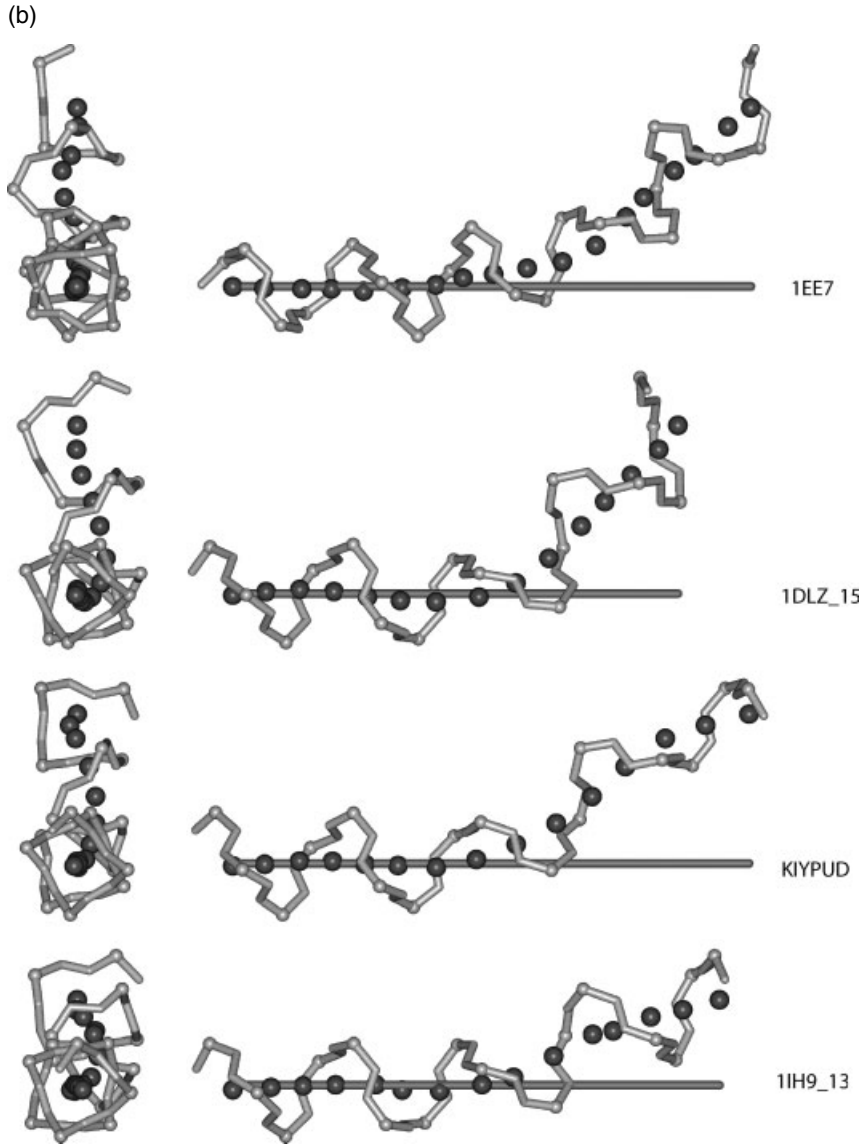

Figure 4b Backbone structure (sticks, Cα atoms: small balls, no oxygen atoms shown), peptide-bond base point of the 3D curvilinear axis (balls) and straight-line axis of peptaibols shown in two orientations rotated by 90°. The database codes are explained in the Introduction.

for ampullosporin A, in these cases different P point pairs have been selected and finally the angle range covering all cases is reported. The ordering of bending angle ranges is (Table 4): zervamicin IIB (isotropic solvent): 11°–26°; alamethicin (chains A and B): 17°–26°; trichotoxin A50E (chains A and B): 32°–36°; [Leu^1]zervamicin: 31°–39°; zervamicin IIB (bound to micelles): 35°–53°; antiamoebin I: 40°–49° (1JOH, chain A), 39°–48° (FEJQOA); chrysospermin C: 40°–42°; ampullosporin A: 53°–64°. The most pronounced difference between literature data and angles derived from the bending graph is found for trichotoxin A50E. Among these structures ampullosporin A exhibits both the strongest bend and a relatively short *C*-terminal segment compared with the length of the straight *N*-terminal subunit. It should be noted here that for trichorzianin TA VII a bending angle of 90°–100° has been reported [12]. As the coordinates are not publicly available, the bending characteristics of this structure cannot be analysed here.

A comparison of the bending angles of zervamicin IIB in an isotropic solvent (1DLZ) and bound to micelles (1IH9) shows that the bending geometry

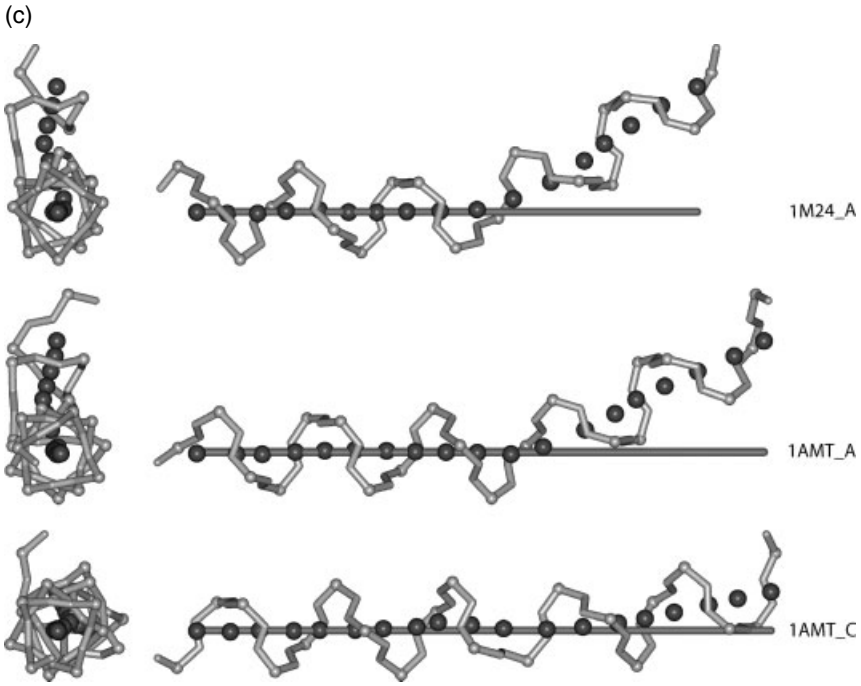

Figure 4c Backbone structure (sticks, Cα atoms: small balls, no oxygen atoms shown), peptide-bond base point of the 3D curvilinear axis (balls) and straight-line axis of peptaibols shown in two orientations rotated by 90°. The database codes are explained in the Introduction.

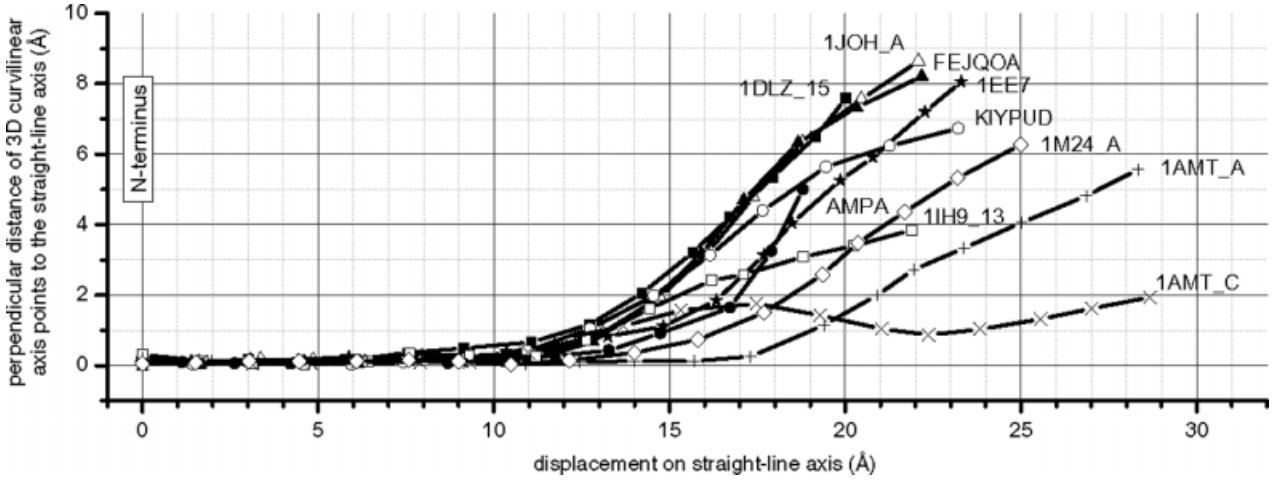

Figure 5 Two-dimensional bending graph for all currently known peptaibol 3D structures: perpendicular distance of peptide-bond base points on the 3D curvilinear axis (spheres) to the straight-line axis obtained from the approximate straight structure parts versus the displacement of the P point projections along the straight-line axis. The least-squares straight-line axes were derived from the following structure parts: AMPA (●) (internal code for ampullosporin A): Ac-Trp^1-Aib^{10}, 1AMT_A (+) (alamethicin, chain A): Ac-Aib^1-Gly^{11}, 1AMT_C (×) (alamethicin, chain C): Ac-Aib^1-Aib^8, 1JOH_A (Δ) (antiamoebin, chain A): Ac-Phe^1-Leu^7, FEJQOA (▲) (antiamoebin I): Ac-Phe^1-Leu^7, 1EE7 (∗) (chrysospermin C): Ac-Phe^1-Aib^{10}, 1M24_A (◊) (trichotoxin_A50E, chain A): Ac-Aib^1-Ala^{10}, 1DLZ_15 (■) (zervamicin IIB in isotropic solvents, all models): Ac-Trp^1-Aib^7, 1IH9_13 (□) (zervamicin IIB in DPC, all models): Ac-Trp^1-Aib^7, KIYPUD (○) ([Leu^1]zervamicin): Ac-Leu^1-Aib^7. Sequence position 1 is always assigned to the first *N*-terminal amino acid. This may differ from the PDB numbering. For 1JOH and 1M24 only chains A are shown in the graph. For 1AMT chains A and C are provided. For 1IH9 and 1DLZ models 15 and 13 are shown, respectively.

Table 4 Geometrical Bending Parameters of Peptaibols[a]

Peptaibol: Database code	Sequence length	Straight *N*-terminal subunit	Bend angle—this work (literature) (°)	Maximum displacement (Å)/ Maximum perpendicular distance (Å)	Cα–Cα distance between first and last residue (Å)
Alamethicin: 1AMT	20				
Chain A		Ac-Aib^{1}-Gly^{11}	22–26 (33) [3]	28.3/5.6	30.0
Chain B		Ac-Aib^{1}-Leu^{12}	17–21	28.3/4.5	30.0
Chain C		Ac-Aib^{1}-Aib^{8}		28.7/1.9	30.4
Ampullosporin A	15	Ac-Trp^{1}-Aib^{10}	53–64	18.8/5.0	20.2
Antiamoebin I: 1JOH	16				
Chain A		Ac-Phe^{1}-Leu^{7}	40–49 (56) [3]	22.1/8.6	24.4
Chain B[b]					24.5
Antiamoebin I: FEJQOA	16	Ac-Phe^{1}-Leu^{7}	39–48	22.2/8.2	24.3
Chrysospermin C: 1EE7	19	Ac-Phe^{1}-Aib^{10}	40–42 (38) [5]	23.3/8.1	25.3
Trichotoxin A50E: 1M24	18				
Chain A		Ac-Aib^{1}-Ala^{10}	34–36 (8) [6]	25.0/6.3	27.1
Chain B		Ac-Aib^{1}-Ala^{10}	32–34 (10) [6]	24.7/5.8	26.9
Zervamicin IIB: 1DLZ[c]	16	Ac-Trp^{1}-Aib^{7}			
Model 17			51–53 (47) [7]	19.0/8.8	20.2
Model 15			44–46	20.0/7.6	20.8
Model 6			35–37	20.7/6.2	21.5
Zervamicin IIB: 1IH9[c]	16	Ac-Trp1-Aib^{7}			
Model 4			24–26[c] (23) [8]	21.4/4.8	22.7
Model 13			17–19	21.9/3.8	23.1
Model 20			11–13	22.0/2.8	23.3
[Leu^{1}]-Zervamicin: KIYPUD	16	Ac-Leu^{1}-Aib^{7}	31–39 (38) [3]	23.2/6.7	24.7

[a] The bending angles were manually determined from the 2D bending graphs using the following peptide-bond base point pairs for the definition of the straight *C*-terminal parts: 1AMT_A (15/16–19/20); 1AMT_B (15/16–19/20); Ampullosporin A (13/14–14/15; 12/13–14/15; 12/13–13/14); 1JOH_A (12/13–13/14; 9/10–15/16); 1EE7 (12/13–18/19); FEJQOA (10/11–14/15; 12/13–14/15); 1M24_A (12/13–16/17); 1M24_B (12/13–16/17); 1DLZ (11/12–15/16); 1IH9 (8/9–15/16); KIYPUD (10/11–12/13; 10/11–14/15). In some cases more than one P point pair has been used. It was assumed that the accuracy of bending angle determination from one P point pair is ±1°. The bending angles for 1AMT and KIYPUD are not taken from the original structure papers but from a paper by Snook *et al.* [3].
[b] For chain B of 1JOH no straight-line axis could be determined.
[c] For the NMR structures 1IH9 and 1DLZ with 20 models each, the data for the most and least strongly bent models are given. The straight *N*-terminal part is identical for all models.

may be very sensitive to the peptide environment. In some cases x-ray structures contain more than one chain in the asymmetric unit. For the two chains of trichotoxin A50E (1M24) and for chains A and B in alamethicin (1AMT) the bending characteristics are similar. On the contrary, chain C of alamethicin is completely different to the other two chains (Figure 5). This demonstrates that the crystal environment also may affect the structures significantly. When using available experimental or theoretical 3D structure information to build ion channel models, this should be properly taken into account.

Conformational Analysis

In molecular mechanics calculations for ampullosporin A, the α-helix with a C_α(Ac-Trp^{1})–C_α(Leu^{15}-ol) interatomic distance of 21.0 Å was found to be around 30 kcal/mol lower in Weiner *et al.* force field energy than the 3_{10}-helix with a C_α(Ac-Trp^{1})–C_α(Leu^{15}-ol) distance of 27.5 Å. For comparison, the x-ray structure shows this distance to be 20.2 Å (Table 4). The sampling of ampullosporin A conformations with MD simulations in a solvent-free environment was started by using a 3_{10}-helix geometry instead of the α-helix in order to avoid the danger of pre-determining the final results by the

starting conformation. Nevertheless, in the 1 ns MD simulation at 340 K, a very fast transition from the 3_{10}-helix to predominantly α-helical structures was observed after about the first 3 ps.

In Figure 6 the calculated α-helical structure with the lowest energy is superimposed on the x-ray structure by using only the α-helical C_α backbone atoms from Ac-Trp^1 to Aib^{13}. The calculated structure is a pure α-helix according to PROMOTIF [30] and is much less bent than the x-ray geometry. A bending analysis was performed of the calculated structure according to the approach described above (data not shown) and it was found that the maximum perpendicular distance is smaller than 1Å compared with 5.0 Å in the x-ray structure (Table 4). From the different bending characteristics of the structure optimized *in vacuo* compared with the x-ray structure it may be concluded that bending is mainly enforced by the crystal environment.

In the following, the entire conformational space sampled in the MD simulations will be analysed. Figure 7 contains three different plots illustrating the results of all the 2500 sampled conformations. The plot of the C_α(Ac-Trp^1)–C_α(Leu^{15}-ol) distance versus the force field energy shows that the majority of the calculated low-energy conformation have a C_α-C_α distance in the range between 20 and 22 Å close to the α-helical structure. Those conformations also cluster together in the factor analysis which is based on all the 28 φ, ψ backbone torsions in addition to the C_α-C_α distance. The x-ray structure is close but somewhat outside this cluster as it is not a pure α-helix. The third graph in Figure 7 separates α-helical from 3_{10}-helical conformations by means of their average plane angles between peptide-bond planes. An ideal 3_{10}-helix will be found at AVER_3_10 of 0° and an α-helix will be found at low AVER_ALPHA values (in the region of 30°). Accordingly, structures with essentially 3_{10}-helices and α-helices will be positioned in the lower right and upper left corner of this plot, respectively.

The plots demonstrate that the conformations with the lowest energy adopt an α-helical structure. As mentioned above short Aib-containing peptides predominantly fold into 3_{10}-helical structures, whereas longer peptaibols containing Aib residues prefer α-helical conformations, but may include 3_{10}-helical stretches. The energy difference between α-helical and 3_{10}-helical conformations seems to decrease with increasing sequence length and may also be dependent on the solvent. For the $(Aib)_{10}$ peptide, for example, this energy difference amounts to −4.3 kcal/mol *in vacuo* and to +0.10 kcal/mol in water [33]. Therefore, it is not totally unexpected that the Weiner *et al.* force field used here favours the α-helix for ampullosporin A in agreement with most parts of the x-ray structure. The effect of the environment on structural characteristics is also found in molecular dynamics simulations on alamethicin [34]. Whereas in a hydrophobic environment there is a simple hinge-bending motion about a proline kink, in water an increased flexibility of the *C*-terminus results in an essentially random-coil conformation being observed. As already mentioned, the difference between the optimized and the x-ray structures at the *C*-terminus may be due to crystal effects. Furthermore, in different solvents or in a changing biological environment, such as in bundles or upon ion channel formation, conformational modifications in the peptaibol might be induced. If the formation of energetically favourable intermolecular interactions required rearranging intramolecular interactions as, for example, established by the internal H-bonding

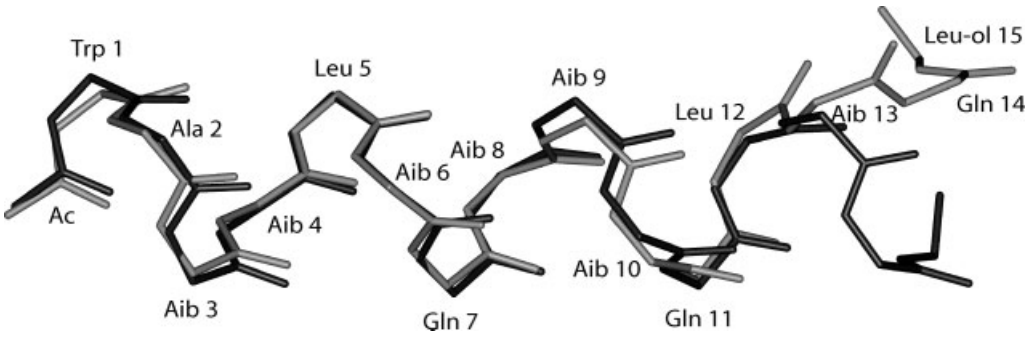

Figure 6 Backbone superposition of the x-ray crystal structure (light grey) and the computed energy-minimum structure (dark grey) of ampullosporin A. Only Cα atoms of the α-helical residue range Ac-Trp^1 to Aib^{13} are used for the alignment. Hydrogen atoms, side chains and solvent molecules are not displayed for clarity reasons.

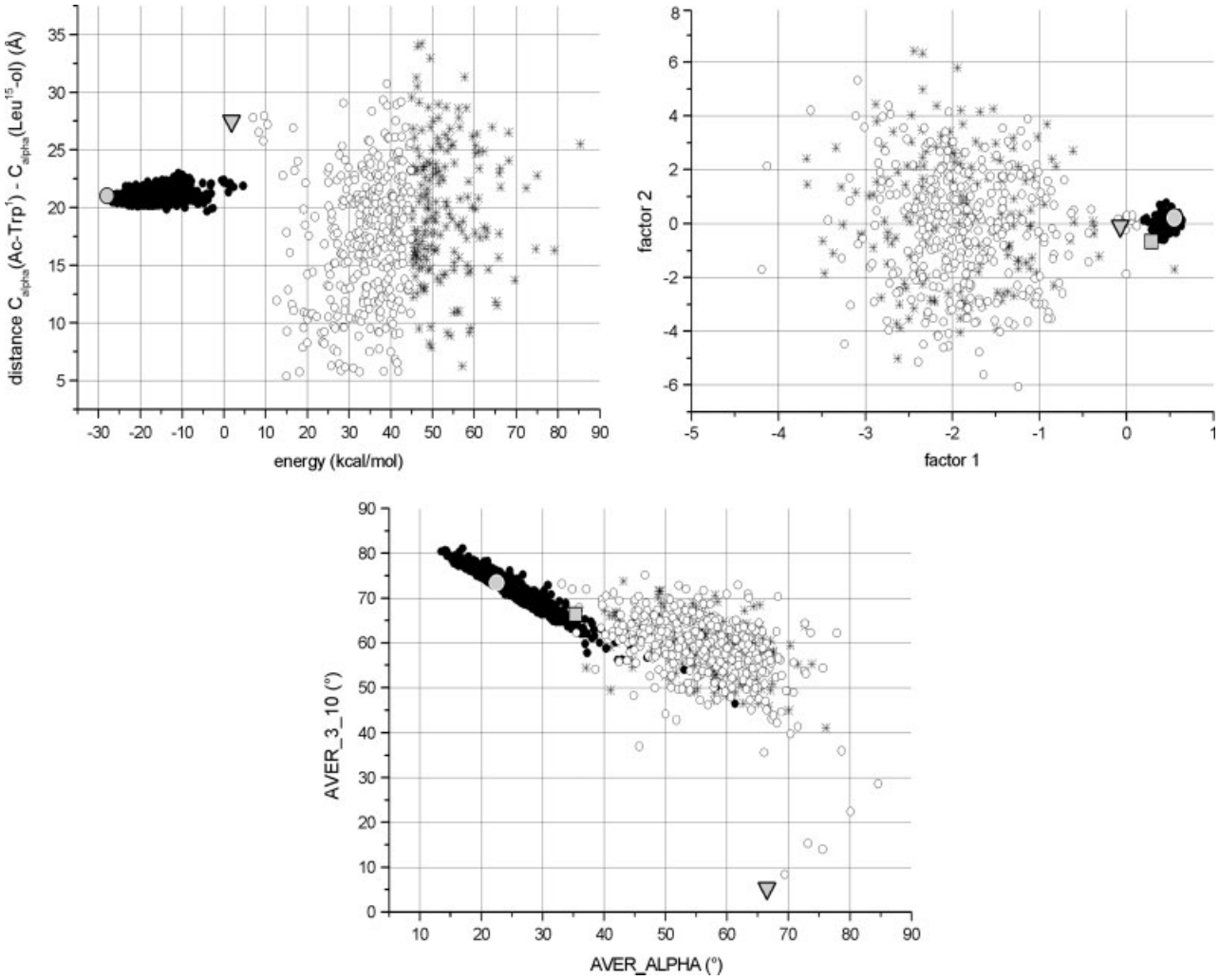

Figure 7 Results of conformational sampling by molecular dynamics simulations. Top: Plot of C_α(Ac-Trp^1)–C_α(Leu^{15}-ol) distance versus the force field energy. Middle: Plot of the two first principal components factor 1 and factor 2 from the factor analysis. Bottom: Average angles between peptide-bond planes (i) and (i + 4) (AVER_ALPHA) versus average angles between peptide-bond planes (i) and (i + 3) (AVER_3_10). The conformations are coded according to the force field energy E: (●) E < +5 kcal/mol, (○) +5 kcal/mol ≤ E < +45 kcal/mol, (∗) ≥ +45 kcal/mol. In addition, the x-ray structure and the optimized α- and 3_{10}-helices are shown as a large grey square, circle and triangle, respectively.

pattern, a different peptaibol conformer as a bioactive conformation may result. In order to model such an arrangement, a better understanding of the atomistic environment of peptaibols in a biological system is needed.

Amphipathicity and Ion Channel Models

Peptaibols are amphipathic molecules, showing a hydrophilic and a lipophilic face. In ampullosporin A the β-carboxylamide groups of Gln^7, Gln^{11} and Gln^{14} contribute to the formation of the hydrophilic side as well as the backbone carbonyl oxygens of Aib^{10} and Gln^{11} that are not involved in intramolecular H-bonds. On the other side, there are the bulky nonpolar side chains of Ac-Trp^1, Leu^5, Leu^{12} and Leu^{15}-ol. This amphipathic characteristic appears to be a prerequisite for ion channel formation [35].

As mentioned above, in a lipophilic environment such as black lipid membranes the ampullosporin A aggregates to form voltage-dependent ion-conducting pores. The x-ray analysis of ampullosporin A has shown that there are some H-bond donor and acceptor sites that are not involved in intramolecular H-bonds (Table 2). These sites can

be assumed to be suitable candidates for helix–helix interactions that are necessary for pore or channel formation. An interesting structural feature is the relatively short length of the C_α(Ac-Trp^1)–C_α(Leu^{15}-ol) distance of ampullosporin A (crystal: 20.2 Å, theoretical α-helical conformations *in vacuo*: 20–22 Å). Therefore, one molecule can hardly span a typical artificial bilayer membrane. But even for such cases different models have been proposed that should enable pore or channel formation and thus membrane activity for short peptaibols [1,11,36–38]. Moreover, peptaibols are known to change their geometry upon channel formation [34,39]. For example, a potential conformational change to a 3_{10}-helix would increase the molecule length of ampullosporin A to about 27 Å. Hence, the length of the molecule in the crystal may not always be identical to the peptide length within an artificial bilayer membrane.

CONCLUSIONS

The single-crystal structure of the 15-meric peptaibol ampullosporin A has been determined as the first solved structure of the peptaibol subfamily SF6. Ampullosporin A is approximately straight between Ac-Trp^1 and Aib^{10} and shows a significant bend of 53°–64° in the *C*-terminal part, although ampullosporin A does not contain any prolines or hydroxyprolines. The secondary structure is α-helical between Ac-Trp^1 and Aib^{13} but less regular with a β-turn characteristic at the *C*-terminus. A new and generally applicable method is described for a quantitative analysis of the bending geometry of peptides or proteins and the results for all currently available peptaibol 3D structures are reported. This procedure includes a 2D bending graph as a novel structure analysis and comparison tool.

Furthermore, a comprehensive molecular dynamics exploration of the ampullosporin A conformational space in *vacuo* is provided. Contrary to the x-ray structure the calculated minimum-energy structure is both almost straight and completely α-helical. This, together with other findings in the experimental structures discussed in this paper, may indicate that the bending characteristics of ampullosporin A and other peptaibols are heavily affected by the actual environment such as solvent effects or crystal forces.

It is often assumed that the formation of voltage-gated channels is related to the various biological activities of peptaibols. To gain deeper insight into the biological effects of ampullosporins much work remains to be done, however. The 3D structure of ampullosporin A reported here is an important step in this direction.

Acknowledgements

We wish to thank Dr H. Sklenar (Max Delbrück Center for Molecular Medicine, Berlin) for making available to us his computer program P-Curve.

REFERENCES

1. Chugh JK, Wallace BA. Peptaibols: models for ion channels. *Biochem. Soc. Trans.* 2001; **29**: 565–570.
2. Fox RO, Richards FM. A voltage-gated ion channel model inferred from the crystal structure of alamethicin at 1.5 Å resolution. *Nature* 1982; **300**: 325–330.
3. Snook CF, Woolley GA, Oliva G, Pattabhi V, Wood SF, Blundell TL, Wallace BA. The structure and function of antiamoebin I, a proline-rich membrane-active polypeptide. *Structure* 1998; **6**: 783–792.
4. Karle IL, Perozzo MA, Mishra VK, Balaram P. Crystal structure of the channel-forming polypeptide antiamoebin in a membrane-mimetic environment. *Proc. Natl Acad. Sci. USA* 1998; **95**: 5501–5504.
5. Anders R, Ohlenschlager O, Soskic V, Wenschuh H, Heise B, Brown LR. The NMR solution structure of the ion channel peptaibol chrysospermin C bound to dodecylphosphocholine micelles. *Eur. J. Biochem.* 2000; **267**: 1784–1794.
6. Chugh JK, Bruckner H, Wallace BA. Model for a helical bundle channel based on the high-resolution crystal structure of trichotoxin_A50E. *Biochemistry* 2002; **41**: 12 934–12 941.
7. Balashova TA, Shenkarev ZO, Tagaev AA, Ovchinnikova TV, Raap J, Arseniev AS. NMR structure of the channel-former zervamicin IIB in isotropic solvents. *FEBS Lett.* 2000; **466**: 333–336.
8. Shenkarev ZO, Balashova TA, Efremov RG, Yakimenko ZA, Ovchinnikova TV, Raap J, Arseniev AS. Spatial structure of zervamicin IIB bound to DPC micelles: implications for voltage-gating. *Biophys. J.* 2002; **82**: 762–771.
9. Karle IL, Flippen-Anderson JL, Agarwalla S, Balaram P. Crystal structure of [Leu^1]zervamicin, a membrane ion-channel peptide: implications for gating mechanisms. *Proc. Natl Acad. Sci. USA* 1991; **88**: 5307–5311.
10. Galbraith TP, Harris R, Driscoll PC, Wallace BA. Solution NMR studies of antiamoebin, a membrane channel-forming polypeptide. *Biophys. J.* 2003; **84**: 185–194.

11. Toniolo C, Peggion C, Crisma M, Formaggio F, Shui X, Eggleston DS. Structure determination of racemic trichogin A IV using centrosymmetric crystals. *Nat. Struct. Biol.* 1994; **1**: 908–914.
12. Condamine E, Rebuffat S, Prigent Y, Segalas I, Bodo B, Davoust D. Three-dimensional structure of the ion-channel forming peptide trichorzianin TA VII bound to sodium dodecyl sulfate micelles. *Biopolymers* 1998; **46**: 75–88.
13. Ritzau M, Heinze S, Dornberger K, Berg A, Fleck W, Schlegel B, Härtl A, Gräfe U. Ampullosporin, a new peptaibol-type antibiotic from *Sepedonium ampullosporum* HKI-0053 with neuroleptic activity in mice. *J. Antibiot. (Tokyo)* 1997; **50**: 722–728.
14. Grigoriev PA, Berg A, Schlegel R, Gräfe U. Differences in ion permeability of an artificial bilayer membrane caused by ampullosporin and bergofungin, new 15-membered peptaibol-type antibiotics. *Bioelectrochem. Bioenerg.* 1997; **44**: 155–158.
15. Kronen M, Kleinwachter P, Schlegel B, Härtl A, Gräfe U. Ampullosporines B,C,D,E1,E2,E3 and E4 from *Sepedonium ampullosporum* HKI-0053: Structures and biological activities. *J. Antibiot. (Tokyo)*. 2001; **54**: 17 517–17 518.
16. Grigoriev PA, Kronen M, Schlegel B, Härtl A, Gräfe U. Differences in ion-channel formation by ampullosporins B, C, D and semisynthetic desacetyltryptophanyl ampullosporin A. *Bioelectrochemistry* 2002; **57**: 119–121.
17. Nguyen HH, Imhof D, Kronen M, Schlegel B, Härtl A, Gräfe U, Gera L, Reissmann S. Synthesis and biological evaluation of analogues of the peptaibol ampullosporin A. *J. Med. Chem.* 2002; **45**: 2781–2787.
18. Grigoriev PA, Schlegel B, Kronen M, Berg A, Härtl A, Gräfe U. Differences in membrane pore formation by peptaibols. *J. Peptide. Sci.* 2003; **9**: 763–768.
19. COLLECT, Data Collection Software; Nonius B.V., Netherlands, 1998.
20. Otwinowski Z, Minor W. Processing of x-ray diffraction data collected in oscillation mode. In *Methods in Enzymology*. Vol. 276. Macromolecular Crystallography, Part A. Carter CW, Sweet RM (eds). Academic Press: San Diego, 1997; 307–326.
21. Sheldrick GM. Phase annealing in SHELX-90: Direct methods for larger structures. *Acta Crystallogr. Sect. A* 1990; **46**: 467–473.
22. Sheldrick GM. SHELXL-97, University of Göttingen, Germany, 1997.
23. Sklenar H, Etchebest C, Lavery R. Describing protein structure: a general algorithm yielding complete helicoidal parameters and a unique overall axis. *Proteins* 1989; **6**: 46–60.
24. SYBYL Software: Tripos Inc., 1699; South Hanley Road, St. Louis, Missouri 63144, USA (www.tripos.com). SYBYL® is a Registered Trademark of Tripos, Inc.
25. Weiner SJ, Kollman PA, Case DA, Singh UC, Ghio C, Alagona G, Profeta Jr S, Weiner P. A new force field for molecular mechanical simulation of nucleic acids and proteins. *J. Am. Chem. Soc.* 1984; **106**: 765–784.
26. Weiner SJ, Kollman PA, Nguyen DT, Case DA. An all atom force field for simulations of proteins and nucleic acids. *J. Comp. Chem.* 1986; **7**: 230–252.
27. Krause K, Pineda LF, Peteranderl R, Reissmann S. Conformational properties of a cyclic peptide bradykinin B2 receptor antagonist using experimental and theoretical methods *J. Peptide Res.* 2000; **55**: 63–71.
28. De Groot BL, Daura X, Mark AE, Grubmüller H. Essential dynamics of reversible peptide folding: memory-free conformational dynamics governed by internal hydrogen bonds. *J. Mol. Biol.* 2001; **309**: 299–313.
29. Toniolo C, Benedetti E. The polypeptide 3_{10}-helix. *Trends Biochem. Sci.* 1991; **16**: 350–353.
30. Hutchinson EG, Thornton JM. PROMOTIF — a program to identify and analyze structural motifs in proteins. *Protein Sci.* 1996; **5**: 212–220.
31. Hummel RP, Toniolo C, Jung G. Conformational transitions between enantiomeric 3_{10}-helices. *Angew. Chem.* 1987; **26**: 1150–1152.
32. Karle I, Balaram P. Structural characteristics of alpha-helical peptide molecules containing Aib residues. *Biochemistry* 1990; **29**: 6747–6756.
33. Zhang L, Hermans J. 3_{10}-Helix *versus* α-helix: a molecular dynamics study of conformational preferences of Aib and alanine. *J. Am. Chem. Soc.* 1994; **116**: 11 915–11 921.
34. Tieleman DP, Sansom MS, Berendsen HJ. Alamethicin helices in a bilayer and in solution: molecular dynamics simulations. *Biophys. J.* 1999; **76**: 40–49.
35. Sansom MS. Alamethicin and related peptaibols — model ion channels. *Eur. Biophys. J.* 1993; **22**: 105–124.
36. Menestrina G, Voges KP, Jung G, Boheim G. Voltage-dependent channel formation by rods of helical polypeptides. *J. Membr. Biol.* 1986; **93**: 111–132.
37. Rizzo V, Schwarz G, Voges KP, Jung G. Molecular shape and dipole moment of alamethicin-like synthetic peptides. *Eur. J. Biophys.* 1985; **12**: 67–73.
38. Wu Y, He K, Ludtke SJ, Huang HW. X-ray diffraction study of lipid bilayer membranes interacting with amphiphilic helical peptides: diphytainol phosphatidylchooline with alamethicin at low concentrations. *Biophys. J.* 1995; **68**: 2361–3269.
39. Cascio M, Wallace BA. Conformation of alamethicin in phospholipid vesicles: implications for insertion models. *Proteins* 1988; **4**: 89–98.

